# A Study of the Effect of Topography on the Merging of Vortices

CHEN Lianshou*[1] (陈联寿), and LUO Zhexian[2] (罗哲贤)

[1] *Chinese Academy of Meteorological Science, Beijing* 100081

[2] *Nanjing Institute of Meteorology, Nanjing* 210044

(Received 28 April 2003; revised 6 September 2003)

**ABSTRACT**

Eight sets of numerical experiments are performed in 48 hours of integtation by using a barotropic primitive equation model with a topographic term so as to investigate the effect of topography on the merging of vortices. It is pointed out that the introduction of topography may change the track of vortices, and it causes the low vortices and vorticity lumps to be detained on the southeast side of the topography, thus creating a favorable condition for the merging of the low vortex and vorticity lumps. It is also shown that the effect of topography may cause double mergers of vortices in a horizontally shearing basic flow, and it can strengthen the low vortex remarkably.

**Key words:** topography, vortex, vortices merger

## 1. Introduction

The merger of vortices is an important issue in vortex dynamics. It has been selected as a first priority research topic in the International Vortex Dynamics Science Symposium held in June 2003. On the other hand, the study on vortex mergers has an operational application value. The regional torrential rain (Deng et al., 1999; Ding, 1993; Gao and Kuo, 1996; Zhu and Chen, 2003a, b) or the rapid intensification of typhoon vortices (Montgomery and Kalenbach, 1997; Moller and Montgomery, 1999; Reasor and Montgomery, 2000) may be all related to the merger of vortices. The authors performed numerical experiments with a barotropic primitive equation model (Chen and Luo, 2003); the results showed that in a shearing basic flow with positive vorticity, the merger of vortex and vorticity lumps may change the monotonously decreasing trend of intensity and increase the vortex sustaining time and its intensity. Gao (1987) indicated that topography is of great importance in the genesis of warm low vortices in southwest China. Our previous paper (Chen and Luo, 2003) did not consider the topographic effect. The topography was introduced into the model in this paper to study its effect on the merger of vortices.

## 2. Model and experiment

### 2.1 *Model and initial/boundary conditions*

The flux form of the barotropic primitive equation is as follows:

$$\frac{\partial u}{\partial t} - v^* q + \frac{\partial}{\partial x}(K + gh) = 0 \,, \tag{1}$$

$$\frac{\partial v}{\partial t} + u^* q + \frac{\partial}{\partial y}(K + gh) = 0 \,, \tag{2}$$

$$\frac{\partial h}{\partial t} + \frac{\partial u^*}{\partial x} + \frac{\partial v^*}{\partial y} + \frac{\partial u_h^*}{\partial x} + \frac{\partial v_h^*}{\partial y} = 0 \,, \tag{3}$$

where $u, v$ are horizontal components of wind velocity, and $h$ is the free surface height.

$$u^* = hu \,,\ v^* = hv \,;\ q = (\xi + f)/h$$

is the potential vorticity, and $K = (u^2 + v^2)/2$ is the kinetic energy.

$$u_h^* = h_{\rm s} u \,,\ v_h^* = h_{\rm s} v \,,$$

and $h_{\rm s}(x, y)$ is the height of topographic surface.

An ideal topography takes the following form:

$$h_{\rm s}(x,y) = \begin{cases} h_0 \sin\dfrac{x - x_1}{x_2 - x_1}\pi \sin\dfrac{y - y_1}{y_2 - y_1}\pi \,, & x_1 \leqslant x \leqslant x_2 \,,\ y_1 \leqslant y \leqslant y_2 \\ 0 \,, & \text{elsewhere} \end{cases} \tag{4}$$

*E-mail: cams@public.bta.net.cn

where we let $x_1$, $x_2$, $y_1$, $y_2$ be far away from the bounds of the computational domain.

With regard to the boundary conditions, on the south and north boundaries $y = 0$ and $D$, we set

$$\frac{\partial u}{\partial t} + \frac{\partial}{\partial x}(K + gh) = 0 \,,$$
$$\frac{\partial h}{\partial t} + \frac{\partial u^*}{\partial x} = 0 \,,$$

which means that there is no flow across the south and north boundaries. On the east and west boundaries, a cyclic boundary condition is used.

With regard to the initial condition, we set

$$h(x,y,0) = h_{\rm V}(x,y,0) + h_{\rm E}(x,y,0) + \sum_{i=1}^{8} h_i(x,y,0) \tag{5}$$

where

$$h_{\rm V}(x,y,0) = \begin{cases} -h_{\rm V0}[1.0 - \exp(-(r_{\rm MV}/r_{\rm V})^b)] \,, & r_{\rm V} < r_{\rm V0} \\ 0 \,, & r_{\rm V} \geqslant r_{\rm V0} \end{cases} \tag{6}$$

$$h_i(x,y,0) = \begin{cases} -h_{i0}[1.0 - \exp(-(r_{{\rm M}i}/r_i)^e)] \,, & r_i < r_{i0} \\ 0 \,, & r_i \geqslant r_{i0} \end{cases} \tag{7}$$

$$h_{\rm E}(x,y,0) = h_{\rm E}(x,y_0,0) + \int (-f/g) u_{\rm E}(y) dy \,. \tag{8}$$

The constant environmental basic flow can be divided into two categories: one is a uniform basic flow

$$u_{\rm E} = u_{\rm E1} \,, \tag{9}$$

and the other is a shearing basic flow

$$u_{\rm E}(y) = -u_{\rm EM} \sin\left(2\pi \frac{y - y_{\rm s}}{W}\right) \,. \tag{10}$$

In formulas (5-10), suffixes V, E, and $i (i = 1, 2, \ldots, 8)$ represent the vortex, the environmental basic flow, and vorticity lumps, respectively, and $h_{\rm V0}$ and $h_{i0}$ are the intensities of the initial low vortex and vorticity lumps. $r_{\rm V} = \sqrt{(x - x_{\rm V0})^2 + (y - y_{\rm V0})^2}$ , $r_i = \sqrt{(x - x_{i0})^2 + (y - y_{i0})^2}$, and $(x_{\rm V0}, y_{\rm V0})$ , $(x_{i0}$ , $y_{i0})$ are the radiuses and central coordinates of the initial low vortex and vorticity lumps respectively. $r_{\rm MV}$ and $r_{\rm Mi}$ are the radius of maximum wind velocity of the vortex and vorticity lumps respectively. $b$ and $e$ are the shape parameters for the vortex and vorticity lumps respectiyely. $r_{\rm V0}$ and $r_{i0}$ denote the radiuses of the initial low vortex and vorticity lumps. $u_{\rm E1}$ represents the uniform basic flow (constant) and $u_{\rm EM}$ is the maximum velocity of the shearing basic flow. $f = 2\Omega \sin\varphi$, $\Omega$ is the rotation rate of the earth, $\varphi$ the latitude, and $g$ the acceleration due to gravity. $u_{\rm E}(y)$ is the zonal wind velocity of environmental flow. $y_{\rm s}$ is the south bound of the computational domain, and $W$ the distance between the south and north bounds.

The initial wind field of the environmental flow is obtained from $h_{\rm E}(x,y,0)$ by using the geostrophic balance relation, and those of the vortex and vorticity lumps are derived from $h_{\rm V}(x,y,0)$ and $h_i(x,y,0)$ by the gradient wind balance relation.

The area of the computational domain is 2000 km×2000 km, containing 201×201 grid points in total. $i = 1, 2, \ldots, 201$, increasing eastwards and $j = 1, 2, \ldots, 201$, increasing northwards. The Arakawa C-grid scheme is used in the Jacobian term, and the Arakawa-Lamb potential enstrophy and energy conserving scheme in spatial difference, and the Nitta-Hovermale scheme in the initialization are adopted.

The parameter values are: $h_{\rm V0} = 180$ m, $h_{10}$ and $h_{50}$ are the free surface height of the first and fifth vorticity lumps at the initial time, $h_{10} = 40$ m, $h_{50} = 2h_{10}$, $\mathrm{h}_{i0}$ $(i = 1, 2, 3, 4, 6, 7, 8) = h_{10}$, $\mathrm{r_{MV}} = 80$ km, $r_{{\rm M}i} = 35$ km $(i = 1, 2, \ldots, 8)$, and $r_{\rm V0} = 320$ km, $r_{i0} = 105$ km; $h_{\rm E}(x, y_0, 0) = 5000$ m, $y_{\rm s} = 0$, $W = 2000$ km, $u_{\rm E1} = u_{\rm EM} = 6$ m s$^{-1}$, $b = 0.5, e = 2.0$. The median line of the computational domain lies on $\varphi$=30°N. The grid spacing is $d = \Delta x = \Delta y = 10$ km, and the time step is $\Delta t = 7.5$ s. The coordinates of the center of the computational domain are (0,0). The coordinates of the center of the initial low vortex are (–500, 500) km; and those of the eight vorticity lumps are successively (–480, 200), (–340, 200), (–200, 200), (–60, 200), (80, 200), (220, 200), (360, 200), and (500, 200) km.

### 2.2 *Experiment design*

Eight experiments were performed, and their parameters are listed in Table1.

**Table 1.** Parameters of the eight experiment.

| Experiment | Intensity of low vortex $h_{V0}$ (m) | Intensity of vorticity lumps $h_{10}$ (m) | Environmental flow | Topographic height $h_0$ (m) |
|---|---|---|---|---|
| 1 | 180 | 0 | Eq. (9) uniform | 0 |
| 2 | 180 | 0 | Eq. (9) uniform | 4000 |
| 3 | 180 | 0 | Eq. (10) shearing | 0 |
| 4 | 180 | 0 | Eq. (10) shearing | 4000 |
| 5 | 180 | 40 | Eq. (9) uniform | 0 |
| 6 | 180 | 40 | Eq. (9) uniform | 4000 |
| 7 | 180 | 40 | Eq. (10) shearing | 0 |
| 8 | 180 | 40 | Eq. (10) shearing | 4000 |

Experiments 1–4 contain no vorticity lumps, and the influence of topography on a vortex in an uniform west wind or shearing basic flow will be analyzed. There are interactions among the low vortex, vorticity lumps, and the environment flow in Expts. 5–8. Under this condition, the effect of topography on a vortex in a straight west wind or shearing basic flow will be analyzed.

## 3. Main results

### 3.1 *Effect of topography on the track of the low vortex*

Under the condition of weak environmental flow, due to the effects of the variation of the Coriolis force with latitude and nonlinear advection, the vortex moves northwestwards (figure omitted). In Expt. 1 there exists an environmental flow of a uniform west wind with a velocity greater than that of the westward shift resulting from the Beta effect, and therefore the vortex moves northeastwards (Fig. 1a). After introducing the topography, the vortex track has a north bias and moves around the north slope of the topography, then turns southeastward (Fig. 1b, Expt. 2). In Expt. 3, there is a horizontally shearing environmental flow expressed by Eq. (10), and the vortex moves slower than in the uniform west wind environmental flow (Fig. 1c). In Expt. 4, it can be seen from comparing Fig. 1d with Fig. 1b that the track of the vortex has a similar bias as that in Expt. 2 in the first 24 h, however in the second 24 h, the movement of the vortex obviously slows down. This is probably related to the distinct decrease in the velocity of the west wind near $y = 400$ km.

In Expts. 5–8, there exists an interaction between the vortex and vorticity lumps. The interaction makes the vortex move northeastwards and slowly (compare Fig. 2a with Fig. 1a and Fig. 2c with Fig. 1c) under the circumstances without topography, but only makes relatively small differences (compare Fig. 2b with Fig. 1b and Fig. 2d with Fig. 1d) under the circumstances with the topography.

The model in this paper contains a low vortex, vorticity lumps, environmental basic flow, and topography. Whether the vortex merges with the vorticity lumps and how they merge are closely related to the change of the vortex intensity. The environmental basic flow provides an environment for the merger of vortices, and the topography indirectly affects the merging via the change of vortex tracks. It can be observed from Figs. 1 and 2 that under the circumstances without topography, the vortex moves northeastwards, and its distances from the vorticity lumps initially on $y = 200$ km (i.e., south and southeast of the vortex, see Fig. 3a) become longer; while under the circumstances with topography, the vortex skirts around the topography, then turns southeastwards, and its distances from the initial vorticity lumps become shorter. Therefore it can be inferred that the topography may affect the merger of vortices.

### 3.2 *Effect of topography on the merger of vorticesnewline in the uniform west wind flow*

In Expts. 5–6, the environmental basic flow is a uniform west wind (Table 1). Although, the initial latitudes of the vortex and vorticity lumps are different, they are transferred eastwards by the basic flow at the same speed.

In Expt. 5 there is no topography. At the initial time, the eight vorticity lumps are arranged from west to east regularly (Fig. 3a), and those lumps form a continuous vorticity band at $t = 4$ h (Fig. 3b). At $t = 8$ h, the vorticity of the band is redistributed, and the band splits up into four vorticity lumps whose scales are larger than the initial one except for the vorticity lump at the southwest end (Fig. 3c). After 4 h, the two lumps in the west end merge together, forming an irregular vorticity-stack area (Fig. 3d). Afterwards, the irregular stack gradually evolves into a circular shape. And at 44 h, it has become an approximately circular

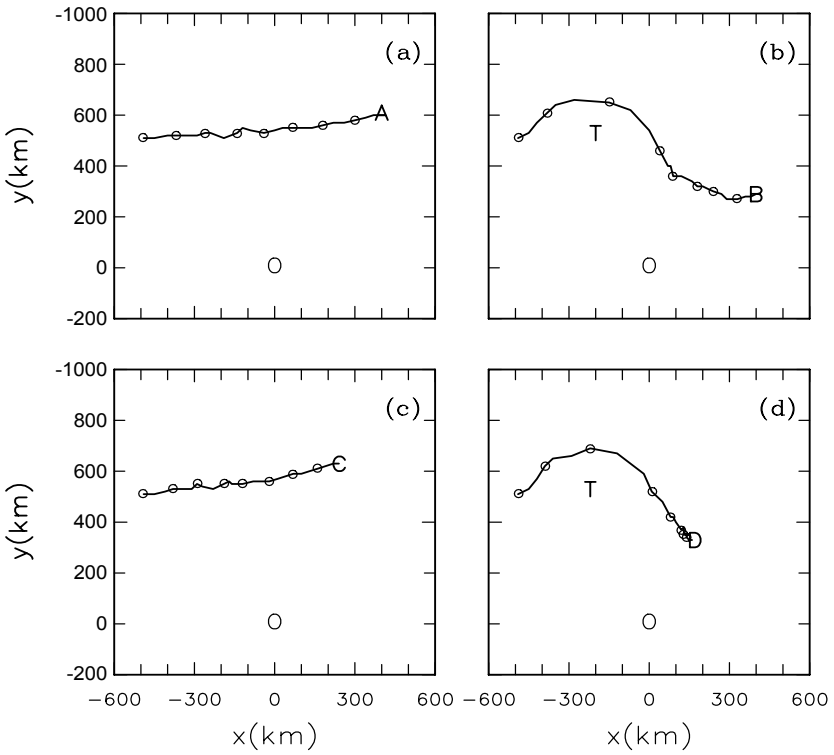


**Fig. 1.** Tracks (marked every 6 h) of the vortex in (a) Expt. 1, (b) Expt. 2, (c) Expt. 3, and (d) Expt. 4. T denotes the center of topography, and O the center of the computational domain.

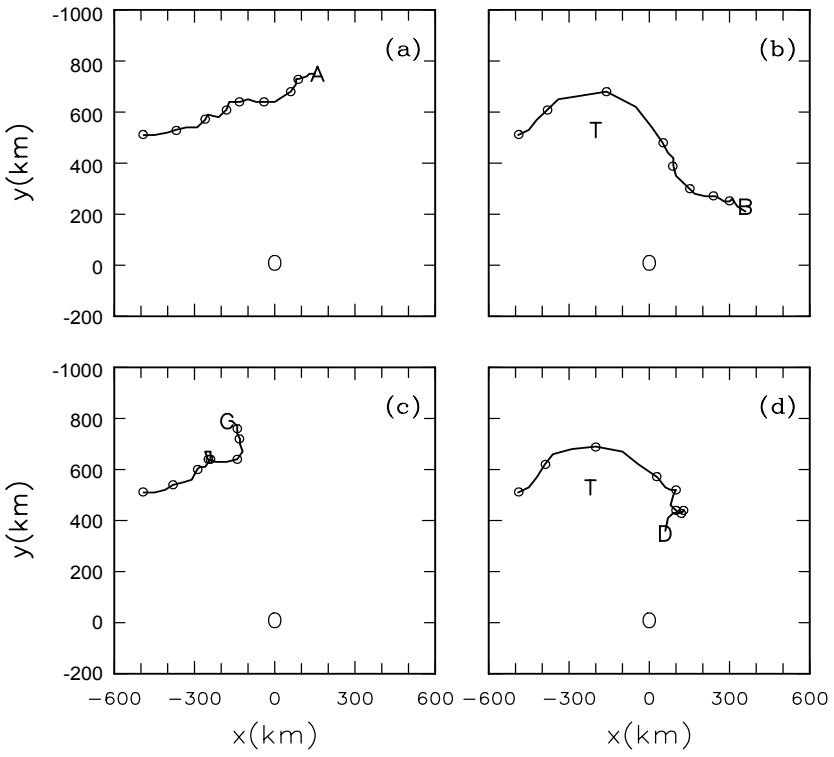


**Fig. 2.** As in Fig. 1, except for (a) Expt. 5, (b) Expt. 6, (c) Expt. 7, and (d) Expt. 8.

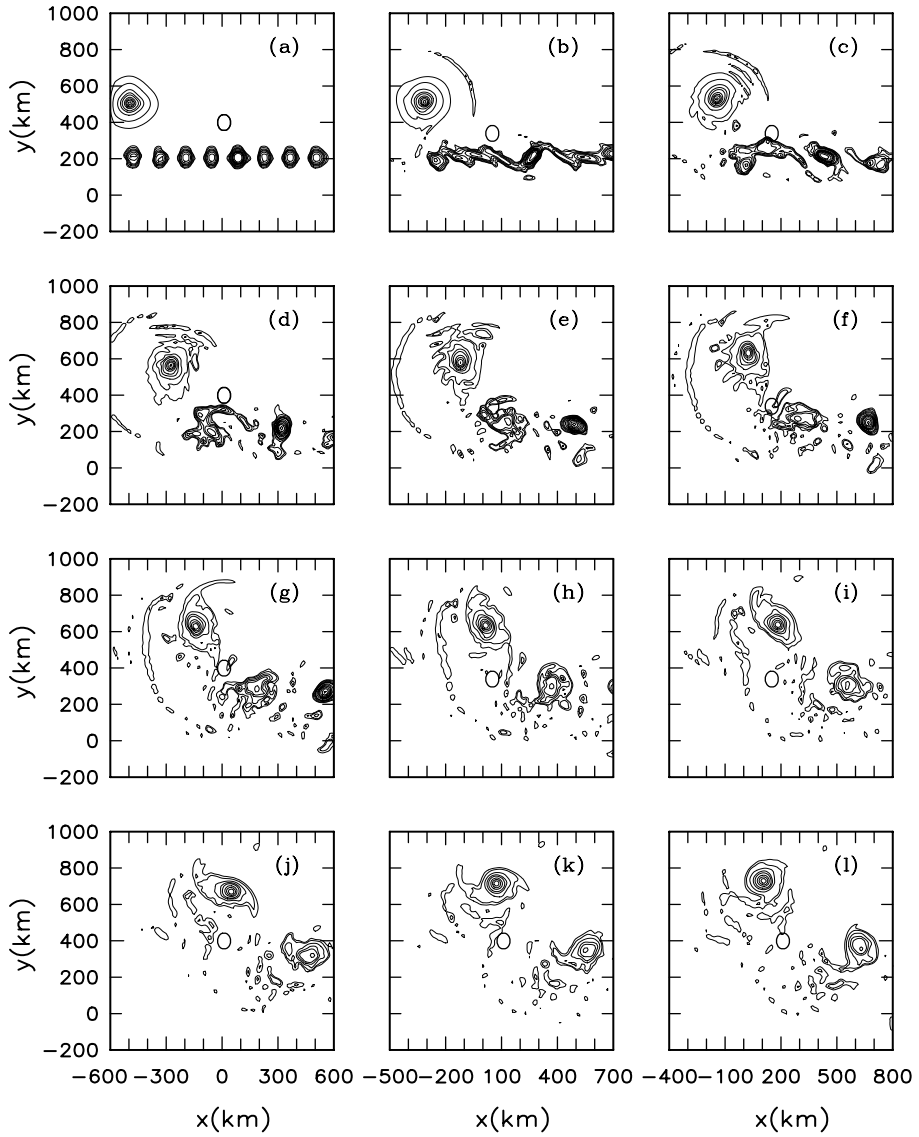


**Fig. 3.** Distributions of relative vorticity during 0–44 h in Expt. 5. (a) 0 h, (b) 4 h, (c) 8 h, (d) 12 h, (e) 16 h, (f) 20 h, (g) 24 h, (h) 28 h, (i) 32 h, (j) 36 h, (k) 40 h, (l) 44 h. The area of the diagram panel is 1200 km×1200 km, and that of the real computational domain is 2000 km×2000 km. The contour interval is $5.0\times10^{-5}$ s$^{-1}$, and the outmost contour of the vortex and vorticity lumps is $5.0\times10^{-5}$ s$^{-1}$.

vortex with spiral bands and with a chaotic distribution area of vorticity on its southwest side (Fig. 3l).

In the period of 12–44 h, there are two points worth mentioning. First, there is no direct merging of the vortex and vorticity band in their eastward movement processes. Secondly, at $t = 16$ h, the vorticity stack is centered in the vicinity of (0, 200) km, and the line between the two centers of the stack and vortex exhibits a NW-SE trend (Fig. 3e); and at $t = 44$ h, the line between the two centers has rotated counterclockwise about 15 degrees. The rotation makes the vortex have a westward component of velocity, which is opposite to the basic flow. Therefore, this may be used to interpret the reduction in the movement of the vortex after introducing vorticity lumps (compare Figs. 1c and 1a).

The center of the vortex at $t = 4$ h (Fig. 4b), 8 h (Fig. 4c), and 12 h (Fig. 4d) in Expt. 6 with topography lies north of the position of the center at the corresponding times in Expt. 5 (without topography) (Figs. 3b, c, d), and the center at $t = 16$ h and 20 h (Figs. 4e, f) lies south of the position in Expt. 5 (Figs. 3e, f). This is due to the fact that the vortex turns

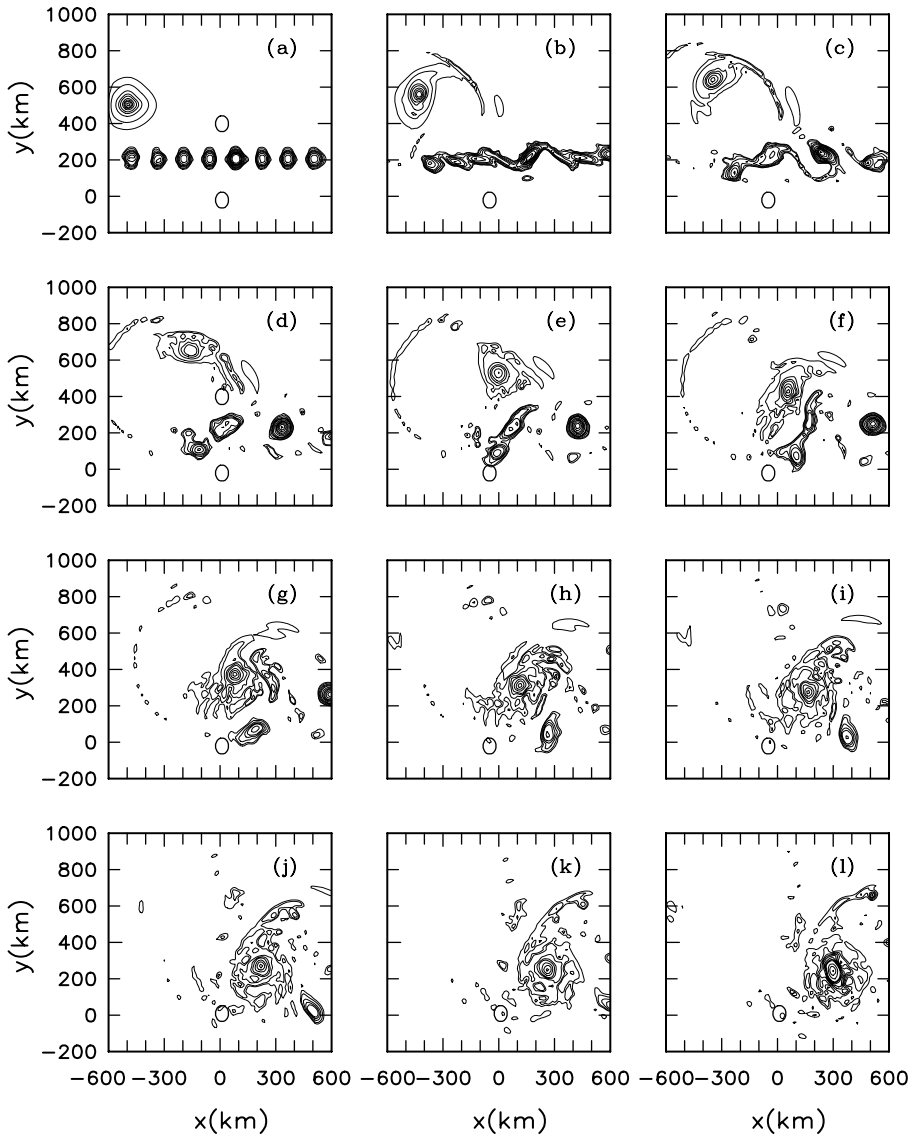


**Fig. 4.** As in Fig. 3 except for Expt. 6.

northeastwards first to skirt around the topography, then turns southeastwards (Fig. 1d), resulting in its merging with the vorticity lumps (Figs. 4g–l). It can be seen from Fig. 4l that the spatial scale of the vorticity-stack area after the merger is larger than that of the initial vortex. Part of the vorticity of the stack comes from the vortex and part of it from the vorticity lumps. At $t = 44$ h in Expt. 5 without topography, there is little vorticity in the vicinity of (300, 200) km, and the main part of the vorticity of the vorticity lump band has moved eastwards to the vicinity of (600, 380) km (Fig. 3l), while in Expt. 6 with topography, the vorticity is concentrated in the vicinity of (300, 200) km (Fig. 4l). This means that under the effect of topography, the vortex is able to organize part of the vorticity lumps, and to cause it to be retained in the southeast of the topography. This result has potential applications to forecast the development of a vortex over a kind of plateau topography due to the merging processes, and needs further investigation.

### 3.3 *Effect of topography on the merger of vortices in a shearing basic flow*

In Expts. 7–8, the environmental basic flow is a horizontal shearing flow (Table 1). The flow in the area $y > 0$ is all west wind, but at different speeds. At the initial time, the center of the vortex lies on the latitude of the maximum west wind $u_{\mathrm{M}}$, and the centers of the

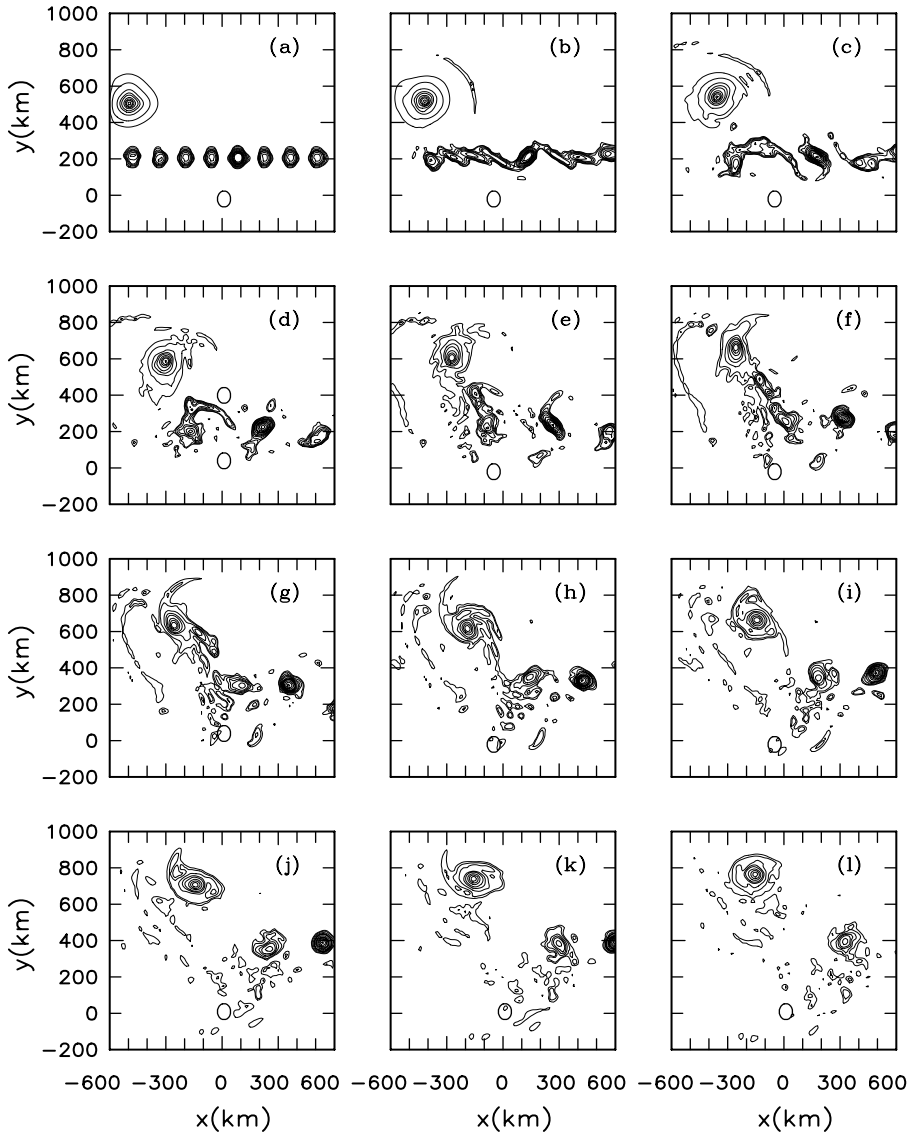


**Fig. 5.** As in Fig. 3 except for Expt. 7.

vorticity lumps lie on the latitude of $0.6u_{\rm M}$. Therefore, the vortex and vorticity lumps are transferred eastwards by the basic steering flow with different velocities.

In Expt. 7 without topography, the situations in the period of 0–12 h (Figs. 5a–d) are similar with those in Expt. 5 (uniform west wind; Figs. 3a–d). A small vorticity lump exists between the vortex and one of the major vorticity lumps in the vicinity of (0, 300) km at 20 h (Fig. 5f), the distance between the vortex and the small lump is decreased at 24 h (Fig. 5g), and at 28 h (Fig. 5h) the small lump has merged into the vortex, thus strengthening the vortex. Afterwards, the vortex maintains an intensity greater than before the merger (compare Figs. 5i–l with Fig. 5d respectively).

In Expt. 8 with topography, in the period of 0–12 h, the eight vorticity lumps separated at the initial time connect with each other and form a vorticity band at first and then the band splits into four new vorticity lumps (Figs. 6a–d); among them the second vorticity lump (lump B) counted from the west boundary is the largest (Fig. 6d). In the next 8 h (Figs. 6e–f), under the effect of the topography, the vortex turns southeastwards and its distance from vorticity lump B is decreased greatly. In the period of 24–32 h, the vortex merges with vorticity lump B (Figs. 6g–i). At $t = 32$ h (Fig. 6i), on the southeast side of the merged vortex there is a stretch of scatted vorticity areas, and on the east side of the area there is a closed vorticity center strengthening at $t = 36$ h (Fig. 6j), and which merges

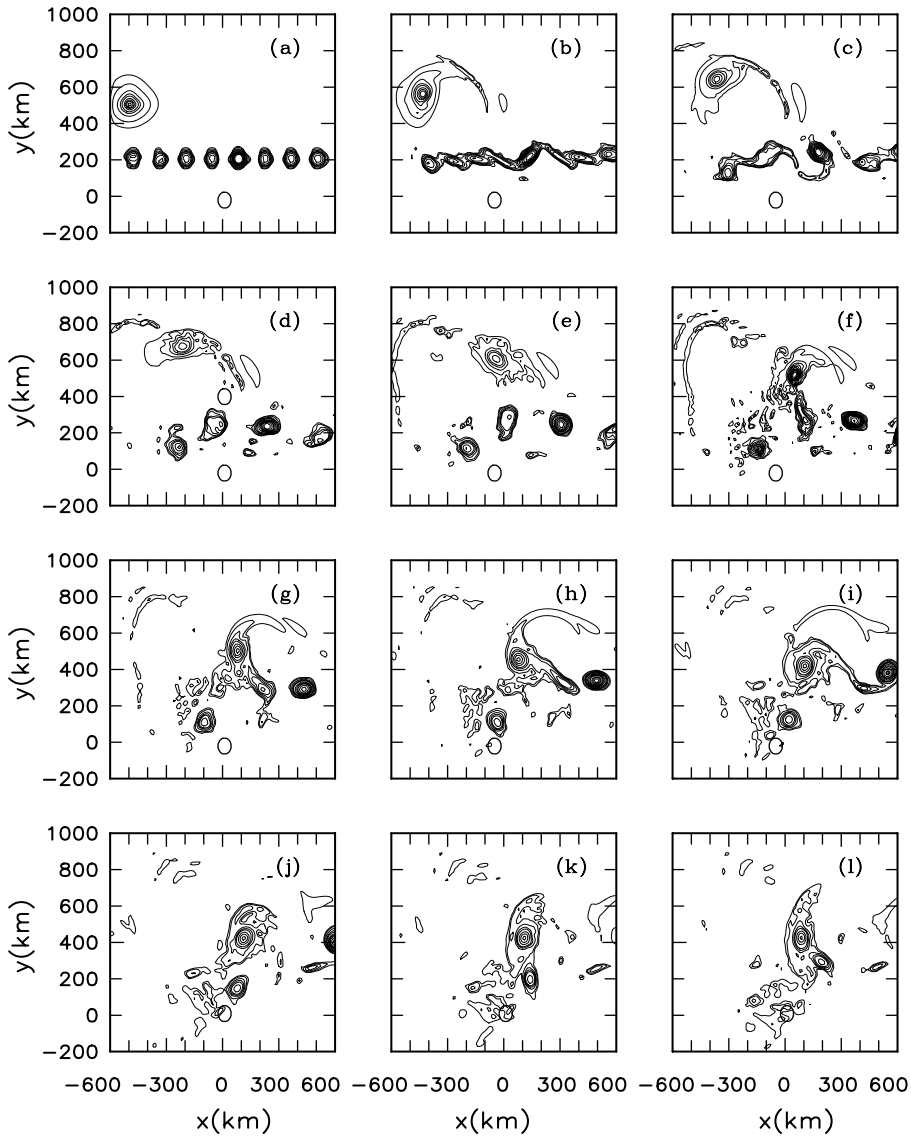


**Fig. 6.** As in Fig. 3 except for Expt. 8.

into the vortex in the period of 40–44 h (Figs. 6k–l). Therefore, the vortex undergoes double mergers with vorticity lumps in its southeastward movement process.

### 3.4 *Effect of topography on the changes in the intensity of the low vortex*

With the linear framework, under the effect of the beta term or a shearing environmental flow, the structure of the vortex which initially has concentric circles and smooth contours may change with time, but the vortex still belongs to a regular pattern of smooth contours. The intensity of the vortex can be represented by the vorticity at its center or the maximum tangential wind speed. On the other hand, within the nonlinear framework, the nonlinear terms may transform a regular pattern of smooth contours into an irregular pattern of unsmoothed contours with a tattered fringe (Luo, 1999). In this circumstance, the vortex can be considered as a spatial structure of the vorticity-stack with irregular distribution. For such a vortex, it is not accurate enough to describe the vortex in terms of the relative vorticity at its center or its maximum tangential wind velocity. The total eddy kinetic energy within the fringe line of a vortex is used in this paper to represent its intensity. The fringe line of a vortex is defined as the outmost contour of vorticity $\xi = 0$. The tangential velocity $V = \sqrt{u^2 + v^2}$ at each grid point within the fringe line of the vortex is calculated at each grid point, and then the sum of eddy kinetic

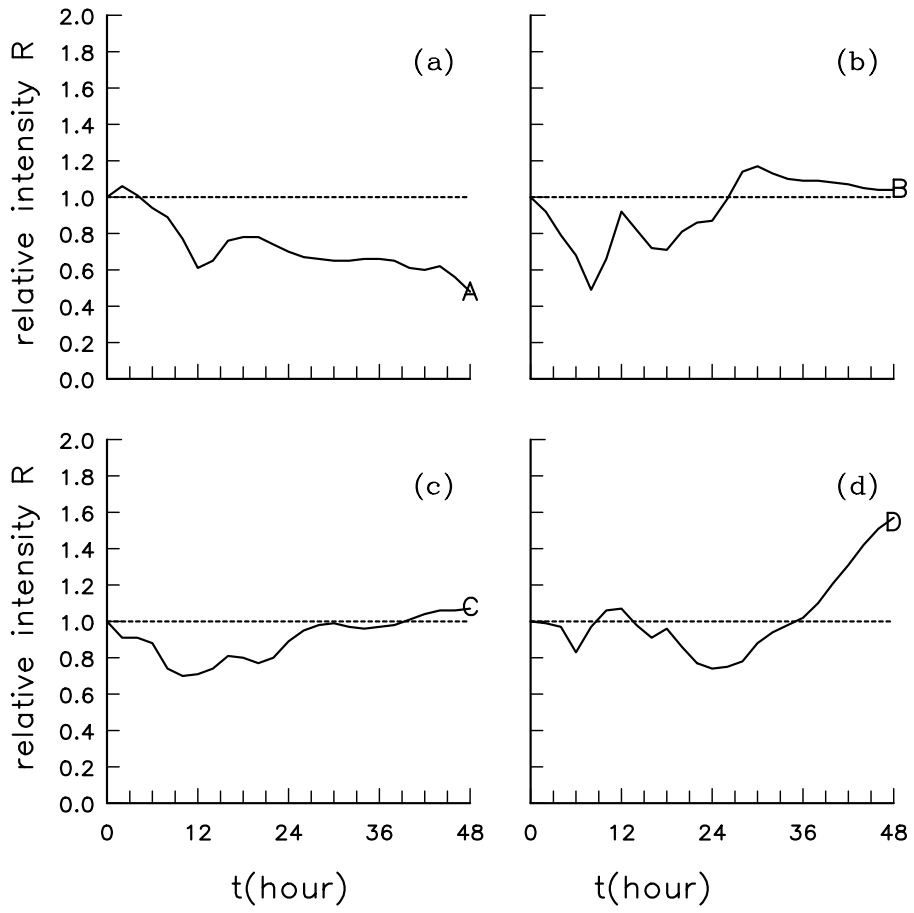


**Fig. 7.** Temporal variations of the relative intensity ($R$) of the vortex in (a) Expt. 5; (b) Expt. 6; (c) Expt. 7; (d) Expt. 8. Dashed lines denote the initial intensity of the vortex.

energy over all grid points within the vortex is computed, where $W_{\rm K} = \sum_{i=1}^{N} \frac{1}{2} V_i^2$, and $N$ is the total number of grid points within the vortex. At last the relative intensity of the vortex, $R = W_{\rm k}(t)/W_{\rm k}(0)$ is obtained, where $W_{\rm k}(0)$ is the total eddy kinetic energy of the vortex at the initial time. $R > (<)1$ represents the strengthening (decay) of the vortex. The above method by which to describe the intensity of a vortex by using the sum of eddy kinetic energy over all grid points within the vortex may have some limitations, which need to be perfected afterwards.

The relative intensities of the vortices $R$ in Expts. 5–8 in the period of 0–48 h are calculated using the above method. As mentioned above, under the conditions of the uniform west wind basic flow and no topography, the vortex and vorticity lumps move eastwards separately without the merging of vortices, and the relative intensity of the vortex decreases with time, i.e., the vortex decays (Fig. 7a, Expt. 5). After introducing the topography, the vortex moving southeastwards merges with the vorticity lumps, thus the relative intensity of the vortex starts to increase at 27h (Fig. 7b, Expt. 6). Under the conditions of a shearing basic flow and no topography, the vortex moves to approach a small lump and merges with it which leads to the relative intensity of the vortex in the period of 24–48 h approximately equaling its initial intensity (Fig. 7c, Expt. 7). In the case with topography (Fig. 7d, Expt. 8), the effect of the topography may cause double mergers with the vortictity lumps, which leads to the vortex strengthening remarkably.

## 4. Conclusion and discussion

During 28–30 July 1998, there were eight cloud clusters over the middle reaches of the Yangtze River. Among them, two clusters merged over Huangshi City of Hubei Province, and another two clusters merged over Wuhan City, producing two exceptionally torrential rains over Huangshi and Wuhan, respectively

(Deng et al., 1999). Those cloud clusters were in accord with the positions of the closed centers of relative vorticity, therefore the merger of the cloud clusters was a problem of the merging of vortices over vorticity fields. Similarly, the merger of a mesoscale vortex with a typhoon is also an important mechanism for the intensification of a typhoon. Therefore, the merging of vortices has drawn much attention from the research community. Chen and Luo (2003) studied this problem and infer that the merging of vortices requires a favorable environment and the adequate inherent conditions. Topography plays an important role in the genesis of the warm low vortex in Southeast China (Gao, 1987). The research results here are actually a supplement to a previous paper (Chen and Luo, 2003) which included no topographic effect.

This paper analyzes the effect of topography on the merging of vortices. In the horizontal shearing basic flow, and the conditions of the adequate disposition of the low vortex and vorticity lumps, the low vortex is only able to maintain its initial intensity without topography, however the vortex may intensify remarkably due to the processes of merging with other vorticity lumps with the effect of topography.

We analyze the merging of vortices only within a framework of ideal topography with a simple model, and therefore the results of this paper are preliminary. It is necessary to study the problem further under the conditions of a more general disposition of the initial vorticity by using a sophisticated model more close to the real atmosphere.

***Acknowledgments.*** This paper was supported jointly by the "973" Project on heavy rain in China, the National Natural Science Foundation of China under Grant No. 40333028, and the Science and Technology Department of China under special project 2001 DIA20026.

## REFERENCES

Chen Lianshou, and Luo Zhexian, 2003: A preliminary study on the dynamics of eastward shifting vortices. *Adv. Atmos. Sci.*, **20**, 323–332.

Deng Qiuhua, Wang Dengyan, Huang Zhiyong, Song Qingcui, and Zhang Ji, 1999: Analyses on the continuous severe heavy rain in southeast Hube in July 1998. *Torrential Rain and Disasters*, No. 1, China Meteorological Press, Beijing, 115–124. (in Chinese)

Ding Yihui, 1993: *Study on the Continuous Exceptational Heavy Rain in the Changjiang-Huaihe River Valley in 1991.* China Meteorological Press, Bejing, 255pp. (in Chinese)

Gao Kun, and Kuo Yinghua, 1996: Study on the predictability of a meso-scale vortex. Studies on Meso-Scale Weather and Dynamics, Ding Yihui, Ed., China Meteorological Press, Bejing, 52–59. (in Chinese)

Gao Shouting, 1987: Effects of streamline fields disposition and topography on the genesis of the warm low vortices in southwest China. *Scientia Atmospherica Sinica*, **11**, 263–271.

Luo Zhexian, 1999: Fractal characteristics of the fringe line of vortices. *Acta Meteorologica Sinica*, **57**, 330–337. (in Chinese)

Moller, J. D., and M. T. Montgomery, 1999: Vortex Rossby waves and hurricane intensification in a barotropic model. *J. Atmos. Sci.*, **56**, 674–687.

Montgomery, M. T., and R. J. Kallenbach, 1997: A theory for vortex Rossby-waves and its application to spiral bands and intensity changes in hurricanes. *Quart. J. Roy. Meteor. Soc.*, **123**, 435–465.

Reasor, P. D., and M. T. Montgomery, 2000: Low-wavenumber structure and evolution of the hurricane inner core observed by air-borne Dual-Doppler Radar. *Mon. Wea. Rev.*, **128**, 653–680.

Zhu Guofu, and Chen Shoujun, 2003a: Analysis and comparison of mesoscale convective systems over the Qinghai-Xizang (Tibetan) Plateau. *Adv. Atmos. Sci.*, **20**, 311–322.

Zhu Guofu, and Chen Shoujun, 2003b: A numerical case study on a mesoscale convective system over the Qinghai-Xizang (Tibetan) Plateau. *Adv. Atmos. Sci.*, **20**, 385–397.